

Electrical properties of heterogeneously doped yttria stabilized zirconia

Binod Kumar^{a,*}, Christina Chen^a, Chakrapani Varanasi^a, Joseph P. Fellner^b

^a *Metals and Ceramics Division, University of Dayton Research Institute, 300 College Park, Dayton, OH 45469-0170, USA*

^b *Propulsion Directorate, Air Force Research Laboratory, Wright-Patterson AFB, OH 45433-7251, USA*

Received 26 July 2004; accepted 15 August 2004

Available online 6 October 2004

Abstract

This paper reports the effects of heterogeneously doped Al_2O_3 on the ionic conductivity of yttria stabilized zirconia (YSZ). At lower dopant concentration, grain growth occurred and the grain boundaries were re-formed. Subsequent increases in the dopant concentration decreased the grain size. The doping leads to the creation of space charge regions in the vicinity of the YSZ– Al_2O_3 boundaries, conducive to enhanced transport of oxygen ions. The presence of Al_2O_3 also leads to a blocking effect. The net result of the two antagonistic influences is small and reflected by a relatively minor influence on conductivity.

© 2004 Elsevier B.V. All rights reserved.

Keywords: Dopant; Zirconia; Ionic conductivity; Microstructure

1. Introduction

Ionic conductivity and microstructure are critical parameters of an electrolyte for its application in a solid oxide fuel cell (SOFC). The ionic conductivity determines, to a large extent, the available power and operating temperature of a SOFC, whereas the microstructure is of vital importance and critical for mechanical properties, including long-term survivability of the electrolyte. The ionic conductivity of a stabilized zirconium oxide depends upon the concentration and mobility of oxygen vacancies, which in turn are closely linked to the dopant concentration. A dopant (Ca^{2+} , Y^{3+} , etc.) concentration higher than the optimum may reduce the number of mobile oxygen ions because of defect association and the resulting ionic conductivity. These homogeneously doped, stabilized zirconia are the mainstay electrolytes in state-of-the-art SOFCs.

The electrical conductivity of stabilized zirconia is explained by the so-called ‘brick layer model.’ [1] The model postulates the existence of cubic grains of stabilized zirconia

uniformly dispersed within homogeneous grain boundaries. The grain boundaries are more resistive than the grains—the grain boundary conductivity (inverse of resistivity) is about two orders of magnitude lower than the grain conductivity. Thus, the bulk conductivity of stabilized zirconia is primarily determined by the weak link, grain boundary conductivity. To improve power density or reduce the operating temperature of a SOFC, the conductivity of the bulk electrolytes needs to be enhanced. To achieve this objective, the grain boundary conductivity must be increased.

A number of different approaches can be employed to enhance conductivity of the bulk electrolyte. For example, a rare earth dopant with an ionic radius closer to the host zirconium, such as scandium, is known to enhance grain conductivity, but the grain boundary conductivity remains unaffected. An alternate route to enhance bulk conductivity of stabilized zirconia is to employ a heterogeneous dopant. These heterogeneous dopants are insoluble in host yttria stabilized zirconia (YSZ) and remain the physically distinct phase of the bulk structure. For a number of ionic conductors, it has been demonstrated that the existence of an inert, heterogeneous dielectric phase in a conducting matrix can raise the ionic conductivity by orders of magnitude [2–8].

* Corresponding author. Tel.: +1 937 229 3452; fax: +1 937 229 3433.
E-mail address: kumar@udri.udayton.edu (B. Kumar).

In a pioneering work, Liang [2] investigated polycrystalline lithium iodide doped with aluminum oxide and reported that lithium iodide doped with 35–45 mol% aluminum oxide exhibited conductivity on the order of $10^{-5} \text{ S cm}^{-1}$ at 25°C , about three orders of magnitude higher than that of the LiI conductivity. However, no significant amount of aluminum oxide was determined to be soluble in LiI; thus, the conductivity enhancement could not be explained by the classical doping mechanism and creation of Schottky defects such as in the LiI–CaF₂ system. Subsequently, a number of investigations have reported enhanced conductivity of silver in the AgI–Al₂O₃ system, [3] copper in the CuCl–Al₂O₃ system, [4] fluorine in the PbF₂–SiO₂ and PbF₂–Al₂O₃ systems, [5] and lithium in polymer–ceramic composite electrolytes [6]. Four review papers [7–10] also document the developmental history and general characteristics of these fast ionic conductors. Analyses of these reviews point out that a new conduction mechanism evolves which augments the bulk conductivity of single-phase ionic conductors. The new conduction mechanism uses interfacial and/or space charge regions between the two primary components. The interfacial or space charge regions are formed because of the creation of charged vacancies and adsorption/desorption of ions. In effect, these regions are electrically active, which influences transport of conducting ions.

The electrical, mechanical, and thermal properties of stabilized zirconia and alumina composites have been studied by a number of investigators [11–16]. Radford and Bratton [11] investigated electrical conductivity of calcia stabilized zirconia (CSZ) containing 2 mol% Al₂O₃. It was found to be insoluble in the CSZ and segregated at the grain boundaries. The addition of Al₂O₃ lowered the electrical conductivity. Verkerk et al. [12] reported the effects of low concentrations of Fe₂O₃, Al₂O₃, and Bi₂O₃ doping on the sintering behavior of YSZ. These dopants were found to have a negative influence on both the grain and grain boundary conductivities. Butler and Drennan [13] analyzed the microstructure of stabilized zirconia as influenced by Al₂O₃ additions. They suggested that Al₂O₃ acted as a scavenger for SiO₂, removing the silicious phase from grain boundary localities. Miyayama et al. [14] reported that up to 0.5 mol% of Al₂O₃ was found to be soluble in stabilized zirconias. They suggested that Al₂O₃ additions have dual roles: below the solubility limit, grain and grain boundary resistivities increase and grain growth is promoted, whereas the reverse is true above the solubility limit of Al₂O₃; i.e., grain boundary resistivity decreases and grain growth is inhibited. However, Miyayama et al. [14] investigated Al₂O₃ additions only up to 1 mol%. Mori et al. [15] characterized mechanical, thermal, and electrical properties of 8 mol% stabilized zirconia with Al₂O₃ doping. The strength of the composites increased with increasing Al₂O₃ content up to 20 wt.%. The thermal conductivity of the composite increased, whereas the coefficient of thermal expansion decreased with increasing Al₂O₃ content. They observed a slight increase in electrical conductivity up to 1 wt.% and subsequently a monotonic decrease with in-

creasing Al₂O₃ content. The electrical conductivity of 8YSZ doped with 20 wt.% Al₂O₃ was reported to be 0.1 S cm^{-1} at 1000°C . The effect of Al₂O₃ additions upon the electrical conductivity of 8 mol% YSZ was also investigated by Feighery and Irvine [16]. They reported that approximately 1 wt.% Al₂O₃ dissolves into the structure of YSZ when sintered at 1500°C for 24 h. Furthermore, the high-temperature conductivity increases for 1 wt.% Al₂O₃ and then decreases to approximately the same conductivity as the undoped 8YSZ. The conductivity remained constant until 10 wt.% Al₂O₃ and subsequently decreased rapidly with further addition of Al₂O₃.

Guo et al. [1,17,18] reported an analysis of the contributions of grain and grain boundaries to the total electrical conductivities of stabilized zirconias. The grain boundaries constituting the core (crystallographic mismatch zone) and space charge regions in stabilized zirconias impede ionic transport across them. The grain boundary resistivity is normally several orders of magnitude greater than the grain resistivity. The resistive grain boundaries have been linked to the impurities, particularly the silicious phase, for a long time. But even in highly pure stabilized zirconias, the grain boundary resistivity was still found to be several orders of magnitude greater than the grain resistivity. Therefore, Guo et al. [18] questioned the proposed origin of the grain boundary resistivity and suggested that the resistive grain boundaries can be explained on the basis of space charges and depletion of oxygen vacancies in the vicinity of grain boundaries. Guo et al. [18] further reported that the addition of Al₂O₃ in small amounts (0.4 mol%) increased both grain and grain boundary resistivities. The grain resistivity was increased by only 3%, whereas the grain boundary resistivity was increased by 600%.

This paper is a culmination of the vast experimental evidence gathered on the role of the heterogeneous doping on the ionic conductivity of composite solids. The effect of nanosized Al₂O₃ doping on the microstructure and conductivity of yttria stabilized zirconia will be investigated, analyzed, and discussed. The Al₂O₃ dopant was selected because of its use in prior literature (although conflicting observations were reported). It is also known to be insoluble in stabilized zirconia in higher concentrations. A large difference in the ionic radii of aluminum and zirconium leads to a very limited solid solubility between the host ZrO₂ and Al₂O₃. Thus, Al₂O₃ is expected to remain a physically distinct phase (heterogeneous) in the bulk structure of stabilized zirconia. By doping with nanosize Al₂O₃, it is expected that the grain boundary resistivity will be affected.

2. Experimental procedure

A quantity of 8 mol% yttria stabilized zirconia obtained from Tosoh Corporation¹ was mixed with nanosize (24 nm)

¹ 4560 Kaisei-Cho, Shinnanyo-shi, Yamaguchi-Ken 746-8501, Japan.

Table 1
Compositions and densities of heterogeneously doped YSZ

Al ₂ O ₃ (wt.%)	Al ₂ O ₃ (mol%)	Density (g cm ⁻³)		Theoretical density (g cm ⁻³)
		1500 °C	1520 °C	
0	0	5.83	5.96	5.96
2	2.56	5.59	5.92	5.92
4	5.10	5.41	5.77	5.88
6	7.60	5.25	5.67	5.84
10	12.53	5.04	5.50	5.76
15	18.53	4.86	5.18	5.66
20	24.37	4.75	5.02	5.56

alumina obtained from NanoTek.² The batch compositions, as shown in Table 1, were mixed in a mortar and pestle and subsequently pressed into discs (1.27 cm in diameter and 0.15 cm thick) with a pressure of 2.5 ton cm⁻² and then sintered at 1500–1520 °C for 4 h. The densities of sintered specimens were measured by the Archimedes principle. The electrical conductivity of each specimen was measured by the ac and dc techniques in the 300–975 °C temperature range. For the ac technique, a Solartron 1260 impedance analyzer with 1287 electrochemical interface was used to obtain impedance data in the 0.1–10⁶ Hz frequency range. The specimen with the highest density for a given composition (corresponding to a sintering temperature of 1520 °C) was characterized by the ac technique. The two surfaces of each specimen were covered with platinum foils and placed in the cell fixture under a pressure applied by tightening the screw of the cell fixture.³ The assembled cell fixture was placed in a furnace and an impedance measurement was conducted as a function of temperature. The dc resistances of these specimens were also measured as a function of temperature using a Fluke multi-meter.

The microstructure was investigated by means of scanning electron microscopy (SEM, JEOL Model JSM-840). The SEM studies were conducted on polished and thermally etched surfaces, and the average grain size was determined by counting the grains and dividing by the area.

A Rigaku Ratablex RV-200BH X-ray diffractometer was used to obtain powder diffraction patterns of the specimens. The sintered specimens were ground into powder and subsequent X-ray diffraction (XRD) patterns were obtained. The diffractometer was operated at 40 kV, 15 mA with copper target.

² Nanophase Technologies Corporation, 8205 S. Cass Ave. #105, Darien, IL 60561.

³ Since all specimens were characterized by the same method, the trend in conductivity variation with composition can be compared and analyzed. The absolute values of the conductivities are expected to be different as compared to the literature, since different experimental conditions were used in the present investigation.

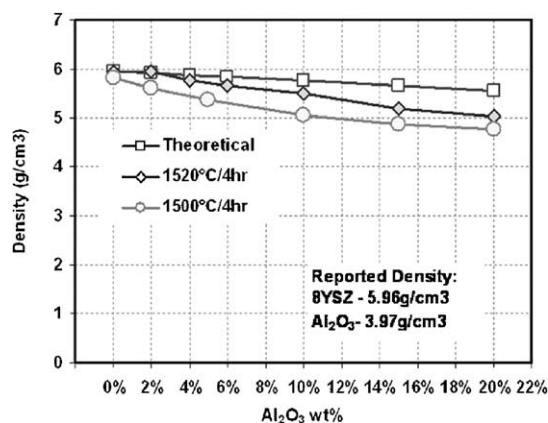


Fig. 1. Density of YSZ vs. wt.% of Al₂O₃.

3. Results and discussion

3.1. Density

Fig. 1 presents plots of theoretical and sintered densities of specimens as a function of Al₂O₃ concentration. Since the density of Al₂O₃, 3.97 g cm⁻³, is lower than the density of the stabilized zirconia, densities of all doped specimens decrease with the concentration of the dopant. An increase in the sintering temperature by 20 °C leads to a significant enhancement in density at all concentrations, with the measured density over 90% of the theoretical density. It is interesting to note that at a 20% dopant level, the electrolyte density is reduced over 16%, which is expected to have a positive influence on the power densities of fuel cell stacks containing these doped electrolytes.

3.2. Microstructure

The microstructures of five specimens containing 0, 4, 6, 10, and 20 wt.% Al₂O₃ are shown in Fig. 2(a–e), respectively. The microstructure of the undoped YSZ (Fig. 2(a)) is typical of the material and shows the presence of pores within the grains. These pores appear as dark, concave spherical regions in the micrograph. The grain boundaries are distinct and do not exhibit the presence of an excessive, segregated impurity

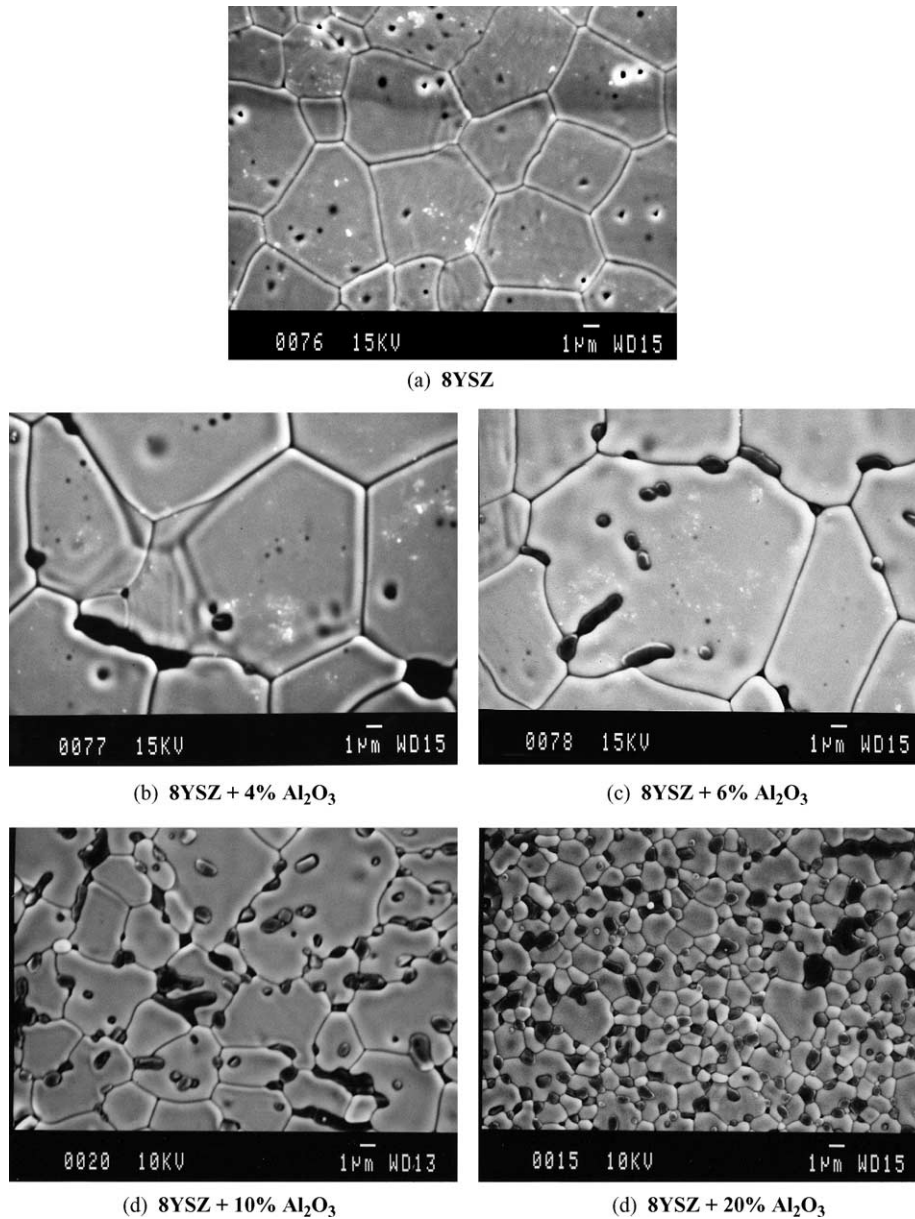


Fig. 2. SEM microstructure of 8YSZ with Al₂O₃ addition from 0 to 20 wt.%.

phase. With the addition of 4 wt.% Al₂O₃, grain growth occurred and the Al₂O₃ phase as shown by the dark areas segregated at the grain boundaries (Fig. 2(b)). The Al₂O₃ precipitates can also be observed inside the grains. The structure of the grain boundaries in Fig. 2(b) suggests that they have been re-formed. The microstructure exhibits well-defined triple points with almost linear grain boundaries. The Al₂O₃ acts as a sintering aid, and the sintering appears to occur by dissolution and precipitation. The solubilities of Al₂O₃ in the YSZ. The excess Al₂O₃ is precipitated primarily at the grain boundaries. Increasing the Al₂O₃ concentration to 6% leads to further grain growth (Fig. 2(c)) and the presence of the

Al₂O₃ phase along the grain boundaries and grain cavity. The presence of Al₂O₃ in cavities is characterized by convex surfaces. At this concentration of Al₂O₃, a linear as well as isolated droplet-like morphology of the dopant are noted. As the concentration of Al₂O₃ increased to 10 wt.%, there is a substantial increase in the volume fraction of this phase (Fig. 2(d)) which exists at grain boundaries and also as distinct grains. The average grain size of the YSZ has been reduced. The 20 wt.% Al₂O₃ specimen (Fig. 2(e)) shows further reduction in the average grain size and the microstructure is on the threshold of transitioning into a nanostructure.

Analyses of all the micrographs shown in Fig. 2(a–e) reveal that the two phases; i.e., YSZ and Al₂O₃, are immiscible

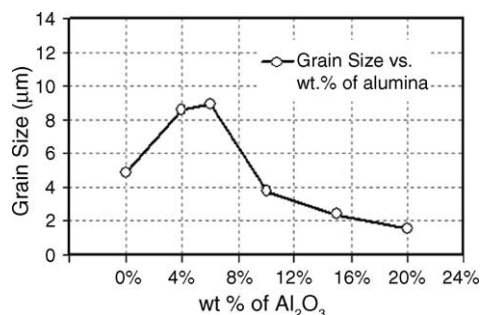


Fig. 3. Grain size vs. Al₂O₃ content (sintered at 1520 °C for 4 h).

at significant concentrations and possess very different surface energies. The Al₂O₃ exhibits non-wettable characteristics on the YSZ substrate.

The average grain size as a function of Al₂O₃ concentration is presented in Fig. 3. As stated earlier, the YSZ grain growth occurs up to about 6 wt.%. This observation is contrary to the reports of Miyayama et al. [14] who observed grain growth until only up to about 0.5 wt.% of Al₂O₃. The dissolution of Al₂O₃ in YSZ in small amounts led to the grain growth. The nanosize Al₂O₃ was introduced to the YSZ. Nonetheless, the size of Al₂O₃ along the grain boundary in the order of several microns in micrographs (Fig. 2(b–c)) may have formed by dissolution, precipitation, and coarsening. Further addition of Al₂O₃ up to 20 wt.% retards grain growth (Fig. 2(d–e)). The 20 wt.% Al₂O₃ material exhibits a morphology with an average grain size of 1.4 µm.

3.3. X-ray diffraction

XRD patterns from undoped and doped (4, 10, and 20%) YSZ are shown in Fig. 4. There is no apparent shift in the d-spacings noted due to the addition of Al₂O₃, which suggests that there is a very limited solid solubility between the

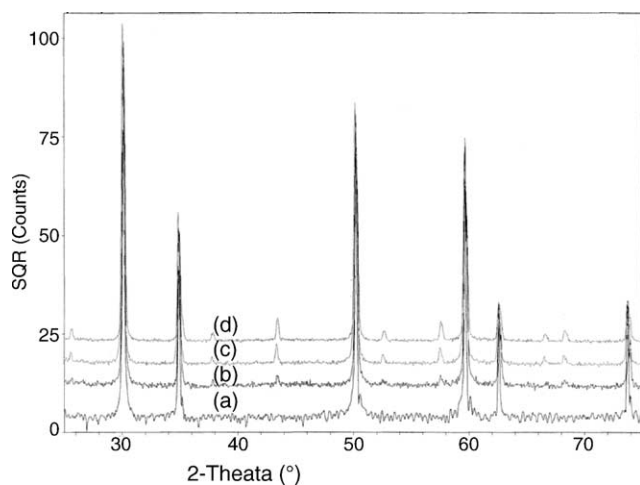


Fig. 4. X-ray diffraction patterns from Al₂O₃ doped YSZ: (a) undoped YSZ, (b) 4 wt.% Al₂O₃-YSZ, (c) 10 wt.% Al₂O₃-YSZ, (d) 20 wt.% Al₂O₃-YSZ.

Table 2
d-Spacings of undoped and doped YSZ

Undoped	Doped		
	4% Al ₂ O ₃	10% Al ₂ O ₃	20% Al ₂ O ₃
2.9614 (YSZ)	2.9616 (YSZ)	2.9698 (YSZ)	2.9611 (YSZ)
2.5649 (YSZ)	2.5669 (YSZ)	2.5712 (YSZ)	2.5648 (YSZ)
	2.3757 (Al ₂ O ₃)	2.3799 (Al ₂ O ₃)	2.3751 (Al ₂ O ₃)
	2.0823 (Al ₂ O ₃)	2.0853 (Al ₂ O ₃)	2.0812 (Al ₂ O ₃)
1.8152 (YSZ)	1.8153 (YSZ)	1.8173 (YSZ)	1.8143 (YSZ)
		1.7399 (Al ₂ O ₃)	1.7369 (Al ₂ O ₃)
		1.6013 (Al ₂ O ₃)	1.5999 (Al ₂ O ₃)
1.5484 (YSZ)	1.5485 (YSZ)	1.5498 (YSZ)	1.5477 (YSZ)
1.4825 (YSZ)	1.4826 (YSZ)	1.4837 (YSZ)	1.4817 (YSZ)
		1.4042 (Al ₂ O ₃)	1.4030 (Al ₂ O ₃)
		1.3737 (Al ₂ O ₃)	1.3722 (Al ₂ O ₃)
1.2839 (YSZ)	1.2841 (YSZ)	1.2850 (YSZ)	1.2842 (YSZ)

two phases. New diffraction peaks corresponding to Al₂O₃ begin to appear in the 4 wt.% specimens and become much stronger for 10–20 wt.% specimens. The d-spacings of these specimens are also presented in Table 2, which clearly shows that the specimens are basically mechanical mixtures of the two components and comply with the definition of heterogeneous doping.

3.4. Oxygen-ion conductivity

A schematic of an equivalent circuit representing a bulk structure of the specimens and corresponding ac impedance response as presented by a plot of real versus imaginary parts of the impedance is shown in Fig. 5. The equivalent circuit consists of a resistor representing contact resistance, a second resistor connected with a capacitor in parallel depicting the ceramic grain and a third resistor with a capacitor in parallel portraying the grain boundaries. The ac response is characterized by the existence of two adjoining semicircles slightly shifted from origin. The magnitude of the shift on the real axis (Z') represents resistance of the electrolyte–electrode contacts. The first semicircle next to the contact resistance depicts the electrical properties (resistance and capacitance)

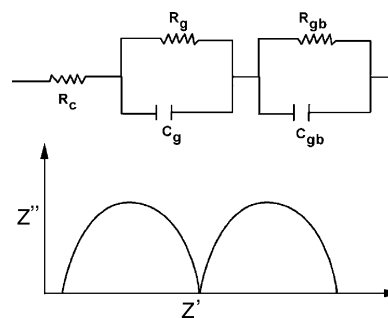


Fig. 5. Schematic equivalent circuit and ac impedance response of a bulk YSZ.

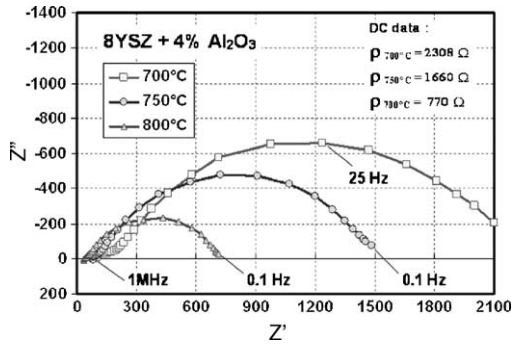


Fig. 6. AC impedance measurement plots at 700–800 °C for 8YSZ + 4% Al₂O₃.

of ceramic grains and the second semicircle represents characteristics of the grain boundary. A simulation study comprised of breadboard circuits and software analysis suggests that the ratio of grain capacitance (C_g) to grain boundary capacitance (C_{gb}) must be less than 10^{-3} for the existence of two semicircles, whereas the ratio of grain resistance (R_g) to grain boundary resistance (R_{gb}) does not matter. If the ratio of $C_g:C_{gb}$ is greater than 10^{-3} , the presence of only one semicircle is predicted.

Typical experimental impedance measurement data for the 4 wt.% Al₂O₃ doped specimen at 700, 750, and 800 °C in the frequency range of 0.1– 10^6 Hz are shown in Fig. 6. The impedance plot is depicted by a distorted semicircle originating from a non-zero origin on the Z' -axis. The temperature increase shrinks the diameter of the distorted circle, illustrating that the specimen becomes less resistive. The resistance value as determined from the diameter of the distorted semicircle on the Z' -axis is also approximately equal to the dc resistance measured by a multimeter (also shown in Fig. 6). The impedance plot of the 10 wt.% Al₂O₃ specimen at 850 °C (Fig. 7) shows three resistance parameters, R_1 , R_2 , and R_{Total} . The R_1 parameter corresponds to the contact resistance whereas $R_2 - R_1$ parameter is the grain resistance. The grain boundary resistance is equal to $R_{Total} - R_2$. These resistances ($R_2 - R_1$ and $R_{Total} - R_2$) were normalized with

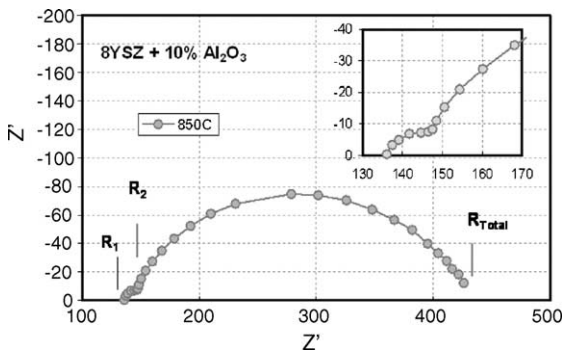


Fig. 7. Determination of resistivities of grain and grain boundary from an ac impedance plot: R_1 is the interface resistance; the grain resistance $R_{grain} = R_2 - R_1$, and the grain boundary resistance $R_{gb} = R_{Total} - R_2$.

specimen geometry (thickness and cross sectional area) to obtain corresponding resistivities (ρ) or conductivities ($\sigma = (1/\rho)$). It should be noted that $R_2 - R_1$ is the diameter of a small semicircle barely discernible (see insert in Fig. 7), implying that the grain possesses both capacitive and resistive elements. The grain boundary of the specimen is characterized by much larger resistive and capacitive elements.

The Arrhenius plots of the grain and grain boundary conductivities of the undoped, 4 and 20 wt.% Al₂O₃ are shown in Fig. 8. It should be noted that the grain conductivity is over an order of magnitude greater than the grain boundary conductivity. The difference between the grain and grain boundary conductivities is less than the value reported for the 8YSZ by Guo et al. [18]. The bulk, total conductivity comprised of grain and grain boundary contributions is shown in Fig. 9. Again in this case the data sets are clustered and it appears that the doping concentration up to 20 wt.% Al₂O₃ has decreased the conductivity; however, the dopant appears to have a minor influence.

The observations on the electrical conductivity of the doped specimens of this investigation parallel the observations made by Mori et al. [15] and Feighery and Irvine [16]. Mori et al. [15] reported that the bulk conductivity of 8YSZ doped with Al₂O₃ increased slightly with increasing Al₂O₃ up to 1 wt.%. Furthermore, they reported that the conductivity of 20 wt.% Al₂O₃ was around 0.1 S cm^{-1} at 1000 °C, about 65% of that of the undoped 8YSZ. Mori et al. [15] had doped the 8YSZ with up to 30 wt.% of Al₂O₃ without observing a major drop in ionic conductivity. Similarly,

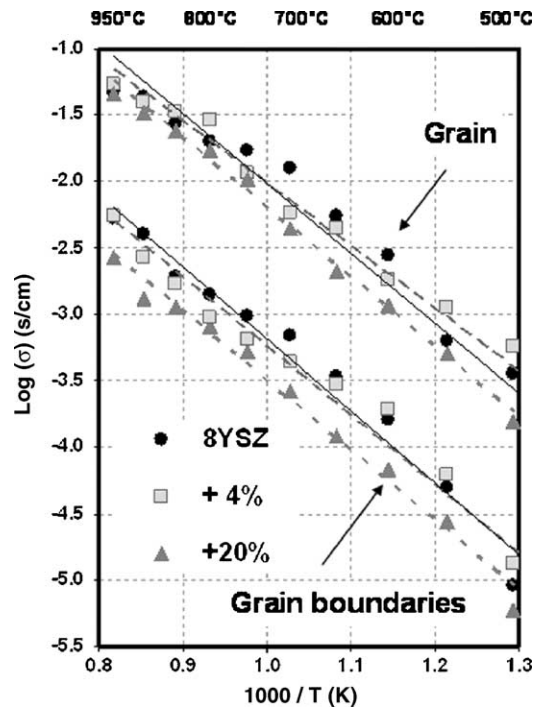


Fig. 8. Conductivity shown as $\log(\sigma)$ vs. $1000/T^{-1}$ for 8YSZ and 8YSZ + 4–20% alumina.

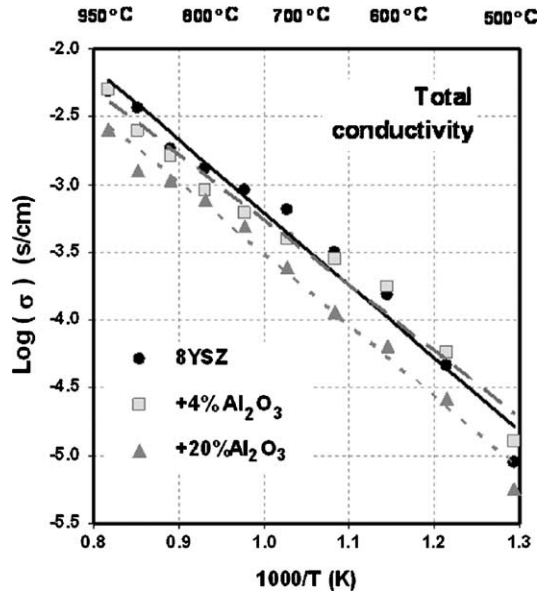


Fig. 9. Arrhenius plots: total conductivity shown as $\log(\sigma)$ vs. $1000 T^{-1}$ for 8YSZ and 8YSZ + 4–20% alumina.

Feighery and Irvine [16] had also doped 8YSZ with Al_2O_3 up to 24 wt.%; however, they reported that 10 wt.% Al_2O_3 can be introduced to the 8YSZ without a significant reduction in the ionic conductivity. Further additions of Al_2O_3 caused a rapid reduction in the conductivity, which was rationalized on the basis of the presence of a large volume fraction of insulating Al_2O_3 phase. Neither Mori et al. [15] nor Feighery and Irvine [16] analyzed contributions of grain and grain boundaries independently on the total bulk conductivity in these heavily-doped YSZ– Al_2O_3 composites.

Since there is a major reduction in the ionically conducting (active) phase in these 8YSZ– Al_2O_3 composites, a normalized plot of ionic conductivity versus Al_2O_3 may be useful to delineate the effect of Al_2O_3 additions. Normalized conductivity (conductivity of a composite/volume fraction of active phase) in S cm^{-1} of grain, grain boundary, and total conductivities is shown in Fig. 10. The normalized grain conductivity shows an enhancement reaching a peak around 15 wt.% of Al_2O_3 . The conductivity enhancement is approximately 30%. The normalized grain boundary conductivity appears to increase initially up to about 4 wt.% and then it gradually decreases. The grain boundary conductivity is lower than the grain conductivity by a factor of 10–15. The bulk total conductivity shows a trend similar to the grain boundary, as it is the dominating factor.

It is of significant relevance to review the effect of inert dopant on the conductivity of an ionically conducting matrix. A general trend on the effect of dopant particles on the ionic conductivity of composites is shown in Fig. 11. With the addition of dopant particles, the ionic conductivity of composites increases and reaches a peak around 20 vol.% of the insulating dopant. Further increases of the dopant decreases the conductivity as it impedes the trans-

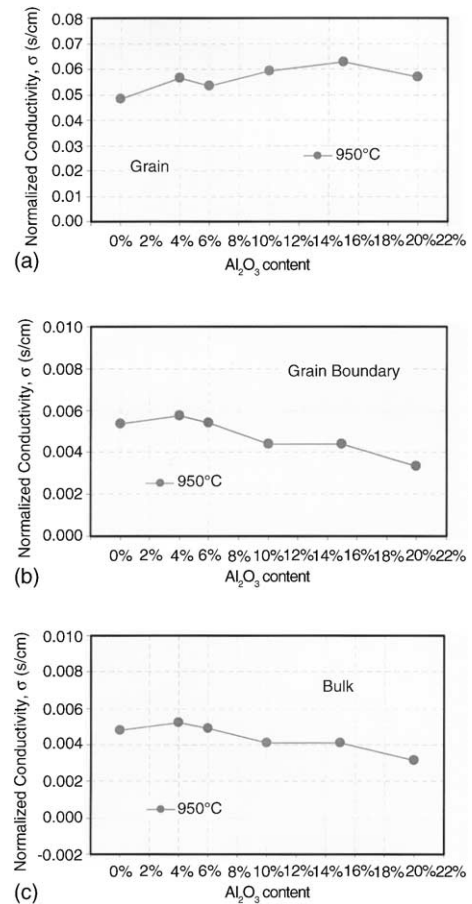


Fig. 10. Normalized conductivity vs. Al_2O_3 content.

port of charged species. A steady-state percolation of the conducting ion occurs around 20 vol.% of the insulating dopant phase leading to an optimum conductivity. The percolation threshold may vary depending upon the matrix dopant chemistries, particle sizes, and processing parameters. The particle size of the dopant has a major influence on the conductivity, which has been reported in earlier publications [6–8].

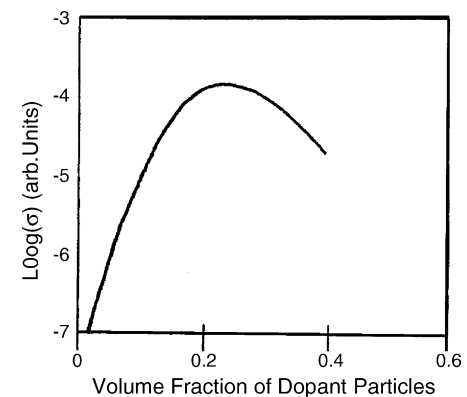


Fig. 11. Low-temperature ionic conductivity of ionically conducting matrix reinforced with insulating particles.

The conductivity data of this investigation does not show a trend characteristic of composite ionic conductors as depicted by Fig. 11 because of: (1) widely different contributions of the grain and grain boundaries to the bulk conductivity of the host material; (2) dissolution, precipitation and grain growth of the dopant phase; and (3) antagonistic influences of the dopant on conductivity. The contributions of grain and grain boundary to total bulk conductivity have been discussed earlier. The dissolution and precipitation of the dopant phase is evident from the microstructures as presented in Fig. 2. Guo and Maier [17] investigated YSZ doped with 0.4 mol% Al_2O_3 in the temperature range of 200–500 °C. Since no Al_2O_3 particles were observed in their SEM images, it was suggested that 0.4 mol% was within the solubility limit. The contribution of Al_2O_3 doping to the grain conductivity was insignificant; however, it drastically decreased the grain boundary conductivity almost by a factor of six. In this investigation, the concentration of Al_2O_3 is much greater and the presence of Al_2O_3 particles primarily at the grain boundaries leads to the formation of space charge regions, which are known to assist transport of charged specie, as in other composite ionic conductors. At the same time, Al_2O_3 particles at larger volume fractions may also impede the transport of the charged specie. Both of these influences on conductivity appear to counteract each other in the specimens investigated in this study. It is known from the work of Guo and Maier [17] that a small amount of Al_2O_3 is detrimental to conductivity. The addition of an excess of Al_2O_3 , which is physically present in the structure, should also hinder transport of the conducting ions. These two factors, therefore, should lead to a rapid drop in the conductivity with Al_2O_3 additions. However, experimental evidence from this investigation and also those of Mori et al. [15] and Feighery [16] are contradictory; thus, one is led to conclude that space charge regions at the YSZ– Al_2O_3 phase boundaries are created which augment the transport of oxygen ions, but a distinct conductivity peak is not observed. Thus, it is suggested that the dopant, Al_2O_3 , imparts antagonistic influences to the total conductivity.

The resistive grain boundary of YSZ results from the depletion of oxygen vacancies, $V_{\text{O}}^{\bullet\bullet}$, in the vicinity of the grain boundaries. A schematic of concentrations of oxygen vacancies, electrons in YSZ, and electrons in Al_2O_3 doped specimens are schematically shown in Fig. 12(a–c). The creation of oxygen vacancies can be expressed by the Kröger–Vink notation:



The depletion of oxygen vacancies near the grain boundary also leads to an enrichment of electron concentration, which provides an energy barrier to the transport of oxygen ions. It is proposed that Al_2O_3 doping reverses Eq. (1) and the electron concentration gradient is removed (Fig. 12(c)). The experimental data in Fig. 10 that the normalized grain boundary conductivity exhibits a slight enhancement in the

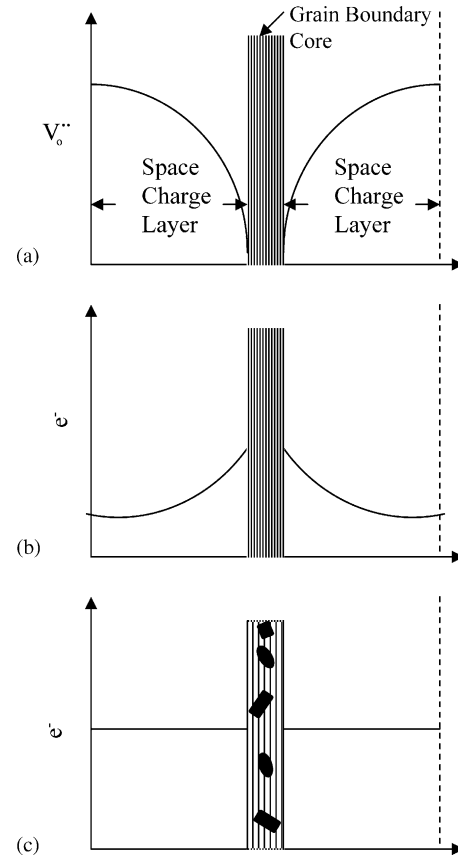


Fig. 12. Schematic profiles of (a) oxygen vacancy, (b) electrons, and (c) electrons in doped YSZ.

early stages of doping and subsequently a gradual reduction attest to the conclusion that the grain boundary conductivity must increase to counteract negative influences of the Al_2O_3 addition.

4. Summary and conclusions

This paper investigated the effects of nanosize Al_2O_3 doping on conductivity of 8 mol% yttria stabilized zirconia. The Al_2O_3 doping concentration was varied from 0 to 20 wt.% and the specimens were characterized by SEM, XRD, and impedance spectroscopy. The significant conclusions of the investigation are summarized as follows:

1. The composite specimens of this investigation were truly heterogeneous as evidenced by SEM micrographs and XRD data. The solid solubility between the YSZ and Al_2O_3 was minimal, as no significant change in the d-spacings occurred.
2. Initially there was a grain growth with the addition of Al_2O_3 up to about 6 wt.%. The grain size increased from 4 to 6 μm and the grain boundaries became sharper. With further addition of Al_2O_3 , the grain size decreased to 1.6 μm for 20 wt. Al_2O_3 .

3. The conductivity data of the bulk specimen obtained from the ac measurement revealed a minor influence on the total, bulk conductivity due to the addition of Al_2O_3 . The conductivity remained relatively flat as the Al_2O_3 content was increased. Both grain and grain boundary conductivities were characterized and their contributions were discussed.
4. The conductivity variation was explained on the basis of antagonistic influences of Al_2O_3 doping. The doping leads to the creation of space charge regions in the vicinity of YSZ– Al_2O_3 boundaries, which should enhance transport of oxygen ions and thus conductivity. The presence of Al_2O_3 may also lead to a blocking effect suppressing conductivity. The net effect of the two antagonist influences is small and reflected by a relatively flat conductivity as the concentration of Al_2O_3 was increased.

Acknowledgment

Three of the authors gratefully acknowledge the financial support by the Air Force Research Laboratory, Propulsion Directorate, under Contract No. F33615-02-D-2299.

References

- [1] X. Guo, Y. Ding, *J. Electrochem. Soc.* 151 (1) (2004) J1–J7.
- [2] C.C. Liang, *J. Electrochem. Soc.* 120 (1973) 1289.
- [3] K. Shahi, J.B. Wagner, *Solid State Ionics* 3/4 (1981) 295.
- [4] T. Jow, J.B. Wagner, *J. Electrochem. Soc.* 126 (1979) 1963.
- [5] K. Hariharan, J. Maier, *J. Electrochem. Soc.* 142 (10) (1995) 3469.
- [6] B. Kumar, S.J. Rodrigues, L.G. Scanlon, *J. Electrochem. Soc.* 148 (10) (2001) 1191.
- [7] R.C. Agrawal, R.K. Gupta, *J. Mater. Sci.* 34 (1999) 1131.
- [8] A. Mikrajuddin, G. Shi, K. Okuyama, *J. Electrochem. Soc.* 147 (8) (2000) 3157–3165.
- [9] P. Knauth, *J. Electroceramics* 5 (2) (2000) 111–125.
- [10] B. Kumar, L.G. Scanlon, *J. Power Sources* 52 (1994) 261.
- [11] K.C. Radford, R.J. Bratton, *J. Mater. Sci.* 14 (1979) 66–69.
- [12] M.J. Verkerk, A.J.A. Winnubst, A.J. Burggraaf, *J. Mater. Sci.* (17) (1982) 3113–3122.
- [13] E.P. Butler, J. Drennan, *J. Amer. Ceram. Soc.* 65 (10) (1982) 474–478.
- [14] M. Miyayama, H. Yanagida, A. Asada, *Am. Ceram. Soc. Bull.* 64 (1) (1985) 660–664.
- [15] M. Mori, T. Abe, H. Itoh, O. Yamamoto, Y. Takeda, T. Kawahara, *Solid State Ionics* 74 (1994) 157–164.
- [16] A.J. Feighery, J.T.S. Irvine, *Solid State Ionics* 121 (1999) 209–216.
- [17] X. Guo, J. Maier, *J. Electrochem. Soc.* 148 (3) (2001) E121–E126.
- [18] X. Guo, W. Sigle, J. Fleig, J. Maier, *Solid State Ionics* 154–155 (2002) 555–561.